

Communication

Beam Steering of a Multi-Port Chassis Antenna Using the Least Squares Method and Theory of Characteristic Modes

Dong-Woo Kim¹, Joon-Hong Kim¹, and Sangwook Nam¹

Abstract—This communication aims to obtain the maximum gain of a multi-port chassis antenna at the desired direction. The beam steering algorithm provides the weighting vector for the multi-port antenna to achieve the above goal. This communication uses the conventional least squares (LSs) method and the theory of characteristic modes (CMs) to find the efficient beam steering algorithm for a multiport chassis antenna. Owing to orthogonal properties of the CMs, the following two advantages emerge: 1) the algorithm provides a simple LS solution without computation of matrix inversion and 2) the physical meaning of this simple LS solution is equivalent to the narrowband time-reversal processing, i.e., phase conjugation processing. Consequently, the proposed algorithm makes it possible to efficiently control the radiation pattern of the multiport antenna in the desired direction with any kind of desired polarization. Validation was conducted by applying the proposed method to an insect-like drone model having three CMs.

Index Terms—Beam steering algorithm, least squares (LSs) method, theory of characteristic modes (TCM), time-reversal processing.

I. INTRODUCTION

Over the last few decades, the topic of a beam steering antenna has been studied to enhance the performance of wireless communication or radar systems. Beam steering to the desired direction helps to increase the reliability of the channel and mitigate the interference, and it has other benefits as well. Typical antennas capable of beam steering include a phased array antenna [1], a reconfigurable leaky-wave antenna [2], and a pattern-reconfigurable single antenna. In a confined space such as within a one wavelength radius, it can be difficult to construct an antenna array and design a leaky-wave antenna. Thus, by proposing the use of a single antenna with a pattern reconstruction capability, efforts have been made to steer the beam in a specific direction within confined spaces [3]–[5].

The theory of characteristic modes (TCM) [6] is one of the useful methods for designing a pattern-reconfigurable single antenna. Basically, the TCM provides the radiation modes of the structure, which are called the characteristic modes (CMs) and are determined by the shape of the structure. This means that the radiation pattern of the pattern-reconfigurable antenna can be represented as a linear combination of the patterns of the CMs. Thus, researchers have tried to analyze and design pattern-reconfigurable antennas in two ways by using the TCM. One approach involves modifying electrical properties of the dominant CMs by using a tunable passive component such as a switch and varactor [7]. However, due to constraints such as the placement of the components and the tunable range of the

actual components, considerable effort is required to achieve the desired beam steering. The other approach is to manipulate the modal weighting coefficient (MWC) of the dominant CMs to achieve the desired current distribution on the investigated platform. This can be done by developing a mode-based multi-port antenna system and adjusting the MWC of the dominant CMs using a beamforming network [8]–[12]. Further, it is important to find an appropriate weighting vector for the desired beam steering for the multi-port antenna. However, most papers to date have focused on coupling element designs and multi-port antenna designs for efficient beam steering and not on algorithms for finding the weighting vector. As some examples for the algorithms, Chen and Wang [8] and Liang *et al.* [9] used random search optimization algorithms such as the genetic algorithm and evolutionary algorithm, which do not guarantee a convergence time for adaptive beam steering and the global optimum for the stated optimization problem. Dicandia *et al.* [10] extracted the relationship between the phase difference and tilt angle by simulations in advance. In [11], the radiation pattern for null steering to the desired angle was implemented based on the concept of the asymmetric CM excitation [12] and solution for a linear equation; however, it did not cover the beam steering.

Therefore, this communication investigates an algorithm for finding a weighting vector for the desired beam steering of a multiport antenna. Among the several algorithms applied for beam synthesis [13]–[17], the conventional least squares (LSs) method is used. Next, the multi-port antenna is assumed to have attributes of decoupling and pure CM generation. Then, the orthogonal properties of the CMs are applied to the LS solution, which results in increasing computational efficiency and stability without calculation of an inverse operator. Importantly, this simplified LSs solution has its own physical meaning. Based on the reciprocity theorem, it turns out that this LS solution satisfies the narrowband time-reversal processing, i.e., phase conjugation processing. Finally, an insect-like chassis model for an unmanned aerial vehicle (UAV), which was already described in [16], and the ideal beamforming network were combined and evaluated with several cases to verify the proposed approach.

The rest of this communication is organized as follows. In Section II, the algorithm for desired beam steering is proposed based on the LS method and the TCM. In Section III, the proposed method is evaluated by using an insect-like multi-port chassis antenna. Finally, the conclusions regarding the findings are given in Section IV.

II. BEAM STEERING ALGORITHM TO THE DESIRED DIRECTION

A. Problem Setup

Consider an N-port chassis antenna with N CMs shown in Fig. 1. Assuming that each port excites one pure CM, and all ports are decoupled, the N-port pattern matrix $\mathbf{A} \in \mathbb{C}^{L \times N}$ by 1 W power excitation can be denoted as

$$\mathbf{A}(\Theta) = \left[\sqrt{e_1} \mathbf{f}_1^{CM}(\Theta) \dots \sqrt{e_N} \mathbf{f}_N^{CM}(\Theta) \right] = \mathbf{A}^{CM}(\Theta) \mathbf{E}_{sq} \quad (1)$$

where $\mathbf{f}_i^{CM}(\Theta) = [f_i^{CM}(\Theta_1) \dots f_i^{CM}(\Theta_L)]^T$ is the E -field radiation pattern of the i th CM; Θ_n represents the direction (θ_n, φ_n) ; e_i is the

Manuscript received October 21, 2018; revised April 30, 2019; accepted May 20, 2019. Date of publication June 6, 2019; date of current version August 12, 2019. This work was supported by a grant to Bio-Mimetic Robot Research Center funded by Defense Acquisition Program Administration, and by Agency for Defense Development (UD130070ID). (Corresponding author: Sangwook Nam.)

The authors are with the School of Electrical and Computer Engineering, Institute of New Media Communication (INMC), Seoul National University, Seoul 152-742, South Korea (e-mail: cb3403@snu.ac.kr; jhkim@ael.snu.ac.kr; snam@snu.ac.kr).

Color versions of one or more of the figures in this communication are available online at <http://ieeexplore.ieee.org>.

Digital Object Identifier 10.1109/TAP.2019.2920288

0018-926X © 2019 IEEE. Personal use is permitted, but republication/redistribution requires IEEE permission.

See http://www.ieee.org/publications_standards/publications/rights/index.html for more information.

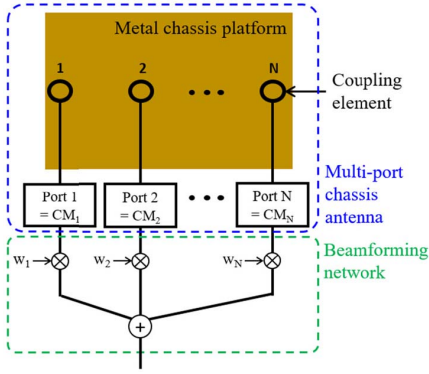


Fig. 1. Systematic configuration of an N-port chassis antenna capable of beam steering.

antenna efficiency of the i th port; $\mathbf{E}_{sq} = \text{diag}(e_1^{1/2}, \dots, e_N^{1/2}) \in \mathbf{R}^N \times N$; and $\mathbf{A}^{CM}(\Theta) = [f_1^{CM}(\Theta) \dots f_N^{CM}(\Theta)] \in \mathbf{C}^L \times N$ is the CM pattern matrix. The synthesized radiation pattern of the N-port chassis antenna $\mathbf{F}(\Theta)$ is presented as

$$\mathbf{F}(\Theta) = \mathbf{A}(\Theta) \mathbf{w} \quad (2)$$

where $\mathbf{w} = [w_1 \ w_2 \ \dots \ w_N]^T \in \mathbf{C}^N$ is the complex weighting vector of the N-port system. Thus, a desired radiation pattern of the N-port chassis antenna $\mathbf{F}_D(\Theta) \in \mathbf{C}^L$ can be determined by finding the proper vector \mathbf{w} given \mathbf{A} satisfying $\mathbf{F}_D(\Theta) = \mathbf{A}(\Theta)\mathbf{w}$. This overdetermined system of linear equations can be approximated by solving the LS problem as follows:

$$\min_{\mathbf{w}} \|\mathbf{F}_D - \mathbf{A}\mathbf{w}\|_2. \quad (3)$$

The LS solution of (3) is well-known as

$$\mathbf{w}_{LS} = [\mathbf{A}^H \mathbf{A}]^{-1} \mathbf{A}^H \mathbf{F}_D. \quad (4)$$

However, it does not provide any physical interpretation and involves two matrix multiplications and one inverse operation that takes the most computational time.

B. Simplification Based on the Orthogonal Property of CMs

One of the well-known properties of CMs is the orthogonality of the radiation pattern presented as

$$\frac{1}{2\eta_0} \int_0^{2\pi} \int_0^\pi f_i^{CM}(\theta, \phi)^H f_j^{CM}(\theta, \phi) \sin \theta \, d\theta \, d\phi = \delta_{i,j} \quad (5)$$

where $\eta_0 = 120\pi$ is the intrinsic impedance in free space. In a discrete domain $\Theta_i = (\theta_i, \phi_i)$, (5) can be rewritten as the following matrix form:

$$(\mathbf{f}_i^{CM})^H \mathbf{S} \mathbf{f}_j^{CM} = \frac{2\eta_0}{\Delta\theta \Delta\phi} \delta_{i,j} \quad (6)$$

where $\mathbf{S} = \text{diag}(\sin(\theta_1), \dots, \sin(\theta_L))$ and $\Delta\theta$ and $\Delta\phi$ are the sampling intervals for θ and ϕ , respectively. Considering the N number of CMs, (6) can be expanded as

$$(\mathbf{A}^{CM})^H \mathbf{S} \mathbf{A}^{CM} = \frac{2\eta_0}{\Delta\theta \Delta\phi} \mathbf{I}. \quad (7)$$

To apply the orthogonal property of CMs, (3) is modified by multiplying $\mathbf{S}^{1/2} = \text{diag}(\sin(\theta_1)^{1/2}, \dots, \sin(\theta_L)^{1/2})$ as

$$\min_{\mathbf{w}} \|\mathbf{F}'_D - \mathbf{A}' \mathbf{w}\|_2 \quad (8)$$

where $\mathbf{F}'_D = \mathbf{S}^{1/2} \mathbf{F}_D$ and $\mathbf{A}' = \mathbf{S}^{1/2} \mathbf{A}$. The LS solution of (8) \mathbf{w}_{LS} is presented as

$$\mathbf{w}_{LS} = [\mathbf{A}'^H \mathbf{A}']^{-1} \mathbf{A}'^H \mathbf{F}'_D. \quad (9)$$

Solution (9) can be simplified as follows using (1) and (7):

$$\mathbf{w}_{LS} = \mathbf{E}_{sq}^{-2} \mathbf{A}' \mathbf{F}_D = \mathbf{E}_{sq}^{-1} (\mathbf{A}^{CM})^H \mathbf{S}^{1/2} \mathbf{F}_D. \quad (10)$$

Compared to (4), solution (10) becomes simple because of the orthogonal property of CMs. The obtained pattern of the chassis antenna $\hat{\mathbf{F}}_D$ is denoted as follows through (10):

$$\hat{\mathbf{F}}_D = \mathbf{A} \mathbf{w}_{LS} = \mathbf{A}^{CM} (\mathbf{A}^{CM})^H \mathbf{S}^{1/2} \mathbf{F}_D. \quad (11)$$

C. Consideration of the Polarization and Phase Values of the Desired Pattern

Considering the polarization, the N-port pattern matrix \mathbf{A} can be rewritten as follows:

$$\tilde{\mathbf{A}}' = \begin{bmatrix} \mathbf{A}'_\theta \\ \mathbf{A}'_\phi \end{bmatrix} = \begin{bmatrix} \mathbf{S}^{1/2} \mathbf{A}_\theta \\ \mathbf{S}^{1/2} \mathbf{A}_\phi \end{bmatrix} = \begin{bmatrix} \mathbf{S}^{1/2} \mathbf{A}_\theta^{CM} \mathbf{E}_{sq} \\ \mathbf{S}^{1/2} \mathbf{A}_\phi^{CM} \mathbf{E}_{sq} \end{bmatrix} = \tilde{\mathbf{S}}^{1/2} \tilde{\mathbf{A}}^{CM} \mathbf{E}_{sq} \quad (12)$$

where subscript θ denotes the θ -polarized component, and ϕ denotes the ϕ -polarized component; $\mathbf{A} = \hat{\mathbf{a}}_\theta \mathbf{A}_\theta + \hat{\mathbf{a}}_\phi \mathbf{A}_\phi$, $\tilde{\mathbf{S}}^{1/2} = \text{diag}(\mathbf{S}^{1/2}, \mathbf{S}^{1/2}) \in \mathbf{R}^{2L \times 2L}$, and $\tilde{\mathbf{A}}^{CM} = \begin{bmatrix} \mathbf{A}_\theta^{CM} \\ \mathbf{A}_\phi^{CM} \end{bmatrix} \in \mathbf{C}^{2L \times N}$. The desired pattern can be rewritten as

$$\tilde{\mathbf{F}}'_D = \begin{bmatrix} \mathbf{F}'_{D,\theta} \\ \mathbf{F}'_{D,\phi} \end{bmatrix} = \begin{bmatrix} \mathbf{S}^{1/2} \mathbf{F}_{D,\theta} \\ \mathbf{S}^{1/2} \mathbf{F}_{D,\phi} \end{bmatrix} = \tilde{\mathbf{S}}^{1/2} \tilde{\mathbf{F}} \quad (13)$$

where $\mathbf{F}_D = \hat{\mathbf{a}}_\theta \mathbf{F}_{D,\theta} + \hat{\mathbf{a}}_\phi \mathbf{F}_{D,\phi}$ and $\tilde{\mathbf{F}} = \begin{bmatrix} p_\theta \mathbf{F}_{D,\theta} \\ p_\phi \mathbf{F}_{D,\phi} \end{bmatrix} \in \mathbf{C}^{2L \times 1}$. p_θ and p_ϕ are the complex constants determined by the desired polarization: $(p_\theta, p_\phi) = (1, 0)$ for θ -polarization, $(p_\theta, p_\phi) = (1, 0)$ for ϕ -polarization, $(p_\theta, p_\phi) = (j, 1)$ for right-hand circular polarization (RHCP), and $(p_\theta, p_\phi) = (1, j)$ for left-hand circular polarization (LHCP). The phase values of $\mathbf{F}_{D,\theta}$ and $\mathbf{F}_{D,\phi}$ were simply set to zero because performance has not been improved herein even though an additional calculation was performed to find an appropriate phase value, such as the iterative LS method [17]. The problem of (8) can be reformulated as follows in the same manner:

$$\min_{\mathbf{w}} \|\tilde{\mathbf{F}}'_D - \tilde{\mathbf{A}}' \mathbf{w}\|_2. \quad (14)$$

The LS solution of (14) \mathbf{w}_{LS} is presented as

$$\mathbf{w}_{LS} = \mathbf{E}_{sq}^{-1} (\tilde{\mathbf{A}}^{CM})^H \tilde{\mathbf{S}}^{1/2} \tilde{\mathbf{F}}_D. \quad (15)$$

The obtained pattern $\hat{\mathbf{F}}_D$ is calculated as follows using (15):

$$\hat{\mathbf{F}}_D = \mathbf{A} \mathbf{w}_{LS} = \tilde{\mathbf{A}}^{CM} (\tilde{\mathbf{A}}^{CM})^H \tilde{\mathbf{S}}^{1/2} \tilde{\mathbf{F}}_D. \quad (16)$$

D. Desired Pattern: Impulse Function

Without considering reality, the ideal desired pattern of a directive antenna is an impulse function in the space domain, which focuses the field only in one direction as

$$\tilde{\mathbf{F}}_D = \begin{bmatrix} p_\theta \delta(\Theta - \Theta_D) \\ p_\phi \delta(\Theta - \Theta_D) \end{bmatrix}. \quad (17)$$

The optimal weighting vector for the LS algorithm is denoted as

$$\mathbf{w}_{LS} = \begin{bmatrix} \frac{\sqrt{\sin(\theta_D)}}{\sqrt{e_1}} (p_\theta f_{1,\theta}^{CM}(\Theta_D)^* + p_\phi f_{1,\phi}^{CM}(\Theta_D)^*) \\ \vdots \\ \frac{\sqrt{\sin(\theta_D)}}{\sqrt{e_N}} (p_\theta f_{N,\theta}^{CM}(\Theta_D)^* + p_\phi f_{N,\phi}^{CM}(\Theta_D)^*) \end{bmatrix} \quad (18)$$

where $*$ is the conjugate operator. The physical meaning of the derived weighting vector can be found using the reciprocity theorem. Considering a plane-wave incoming from the angle $\Theta_D = (\theta_D, \phi_D)$ with the polarization of (p_θ, p_ϕ) , the received signals for the N-ports correspond to the scaled values of the radiation patterns as

$$\mathbf{r} = \begin{bmatrix} A\sqrt{e_1}(p_\theta^* f_{1,\theta}^{CM}(\Theta_D) + p_\phi^* f_{1,\phi}^{CM}(\Theta_D)) \\ \vdots \\ A\sqrt{e_N}(p_\theta^* f_{N,\theta}^{CM}(\Theta_D) + p_\phi^* f_{N,\phi}^{CM}(\Theta_D)) \end{bmatrix} \quad (19)$$

where $A \in \mathbb{C}$ is the signal strength of the incoming plane-wave. Comparing (18) with (19), the derived weighting vector is the same as the phase conjugation of the received signal \mathbf{r} . In other words, the weighting vector by the proposed algorithm is equivalent to the time-reversal processing of the narrowband received plane-wave signal.

E. Desired Pattern Considering the Beam Solid Angle

Because of the finite aperture size of the antenna, the beam synthesis mainly was performed to obtain the desired pattern considering beamwidth [13]–[17]. This approach considering the beam solid angle can also be applied to the proposed algorithm using the following function:

$$\tilde{\mathbf{F}}_D = \begin{bmatrix} p_\theta \mathbf{1}_K(\Theta) \\ p_\phi \mathbf{1}_K(\Theta) \end{bmatrix} \quad (20)$$

where $\mathbf{1}_K = \sum_{k \in K} e_k$ is the sum of the unit vectors for the set $K \subset \{k | (\theta_D - \theta_{W1}, \phi_D - \phi_{W1}) \leq \Theta_k = (\theta_k, \phi_k) \leq (\theta_D + \theta_{W2}, \phi_D + \phi_{W2}), k \in \mathbb{R}\}$, and θ_W and ϕ_W are determined by the chosen beam solid angle. The optimal weighting vector for the LS algorithm is presented as follows:

$$\mathbf{w}_{LS} = \begin{bmatrix} \sum_{k \in K} \frac{\sqrt{\sin(\theta_k)}}{\sqrt{e_1}} (p_\theta f_{1,\theta}^{CM}(\Theta_k)^* + p_\phi f_{1,\phi}^{CM}(\Theta_k)^*) \\ \vdots \\ \sum_{k \in K} \frac{\sqrt{\sin(\theta_k)}}{\sqrt{e_N}} (p_\theta f_{N,\theta}^{CM}(\Theta_k)^* + p_\phi f_{N,\phi}^{CM}(\Theta_k)^*) \end{bmatrix} \quad (21)$$

Compared (21) with (18), the weighting vector for the desired pattern is the weighted sum of the weighting vector for the impulse desired pattern. In other words, the weighting vector for this desired pattern is equivalent to time-reversal processing of the weighted sum of the narrowband received plane-wave signals from the angle between $(\theta_D - \theta_{W1}, \phi_D - \phi_{W1})$ and $(\theta_D + \theta_{W2}, \phi_D + \phi_{W2})$. Compared to the impulse desired pattern mentioned in Section II-D, the result of the time-reversal processing averaged for the wide angle may lead to a decrease in the maximum beam steering performance.

III. VERIFICATION OF THE PROPOSED BEAM STEERING ALGORITHM

A. Introduction of the Multi-Port Antenna and Data Extraction

An insect-like chassis model for a UAV, which was already explained in [18], was used to evaluate the proposed method. As shown in Fig. 2, the insect-like chassis model has three dominant CMs with modal significances of 0.98, 0.92, and 0.38 at 2.4 GHz. Each modal pattern has both θ - and ϕ -polarized components. As shown in Fig. 3, using the symmetric properties and mode decoupling network, the three-port chassis antenna was implemented with the characteristics of being able to generate a pure individual CM per port and a low coupling ratio less than -20 dB. Each port had a total antenna efficiency of 59.5%, 90.7%, and 73.2% in the

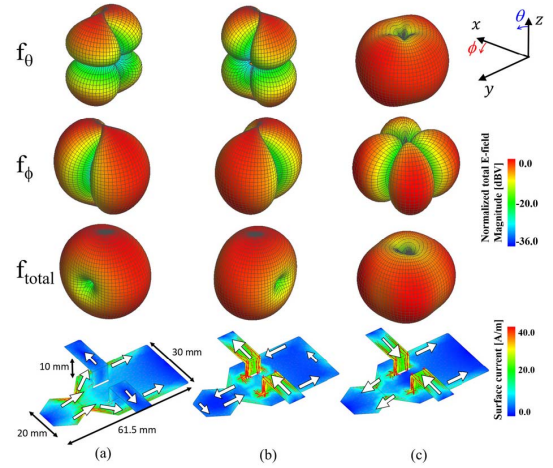


Fig. 2. Simulated normalized radiation patterns and surface current distribution of the first three dominant CMs of the platform at 2.4 GHz [18]. (a) Mode 1. (b) Mode 2. (c) Mode 3.

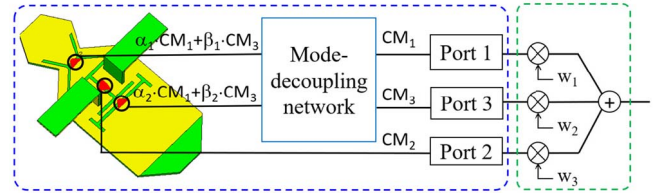


Fig. 3. Configuration of the insect-like three-port chassis antenna and its ideal beamforming network.

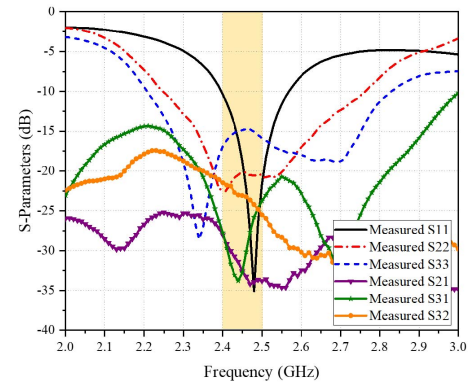


Fig. 4. Measured S-parameters of the insect-like three-port antenna system [16].

simulations and 51.2%, 83.6%, and 52.9% in the measurements. The readers are referred to the detailed description of this antenna in an earlier work [18]. A beamforming network that can be designed in the radio frequency (RF)/analog domain or digital domain can be used to steer the beam pattern without a problem because of the decoupling and 50Ω matching characteristics of the multiport antenna system in Fig. 4.

In this verification, the E -field pattern matrix by 1 W excitation was obtained at intervals of 5° for $\theta \in [0^\circ, 180^\circ]$ and $\phi \in [0^\circ, 360^\circ]$, thereby resulting in $\tilde{\mathbf{A}}$ with a dimension of 5402×3 . After extracting $\tilde{\mathbf{E}}_{sq}$ and $\tilde{\mathbf{A}}^{CM}$ based on (1) and (7), the weighting vector and the resulting pattern can be obtained by the LS algorithm mentioned in the previous section once the desired pattern is designed.

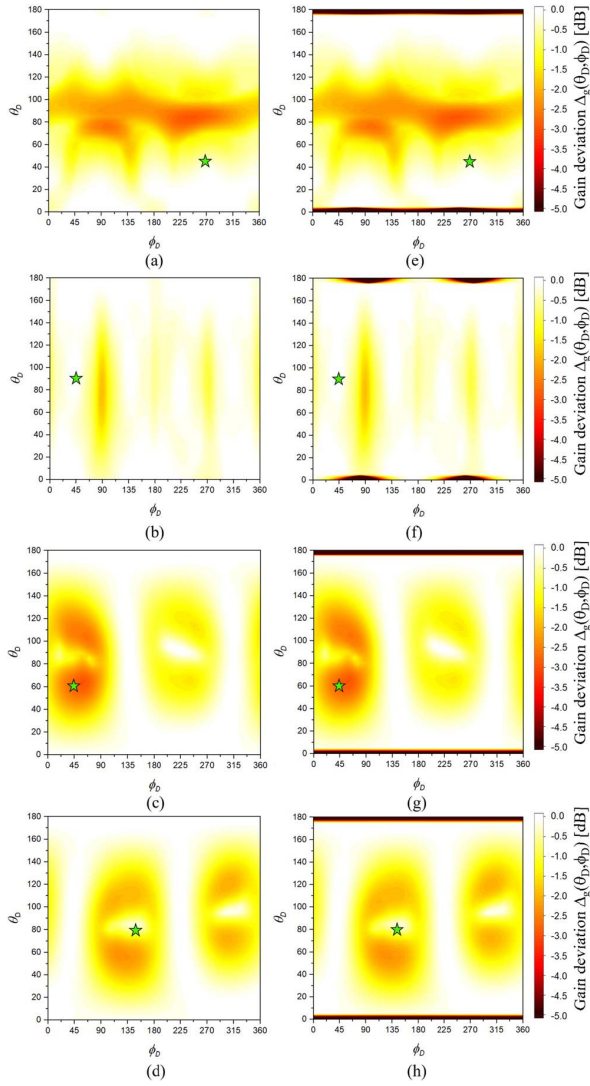


Fig. 5. (a)–(d) Investigation of the capability of the proposed beam steering algorithm for the impulse desired pattern. (e)–(h) Desired pattern considering beam solid angle. The gain deviations (22) for all angles at an interval of 5° are investigated for the following polarizations. (a) and (d) θ polarization. (b) and (f) ϕ polarization. (c) and (g) Right-handed circular polarization. (d) and (h) Left-handed circular polarization. For the cases marked with an asterisk, the radiation patterns are provided in Fig. 6.

B. Numerical Beam Steering Results for the Multi-Port Antenna

The validation was verified by calculating and visualizing the numerical beam steering results in MATLAB [19]. The numerical beam steering was conducted in detail by synthesizing the ports' radiation patterns in an ideal beamforming network, whose weighting vector was determined by the proposed algorithm. The beam steering capabilities for all the angles were investigated in Fig. 5 by visualizing the following gain deviation between the maximum copolarized gain and the copolarized gain for the desired direction (θ_D, ϕ_D)

$$\Delta_g(\theta_D, \phi_D) = 20 \log \left(\frac{|\hat{\mathbf{F}}_{co}(\theta_D, \phi_D)|}{\text{Max}(|\hat{\mathbf{F}}_{co}|)} \right) \quad (22)$$

where subscript “co” indicates the copolarized value, and $\text{Max}(\cdot)$ extracts the maximum value of the entry in the vector (\cdot) . The values of Δ_g range from 0 to $-\infty$, and the value will be zero when the beam pattern perfectly steers to the desired direction. The proposed beam steering algorithm was performed for all polarizations and angles at

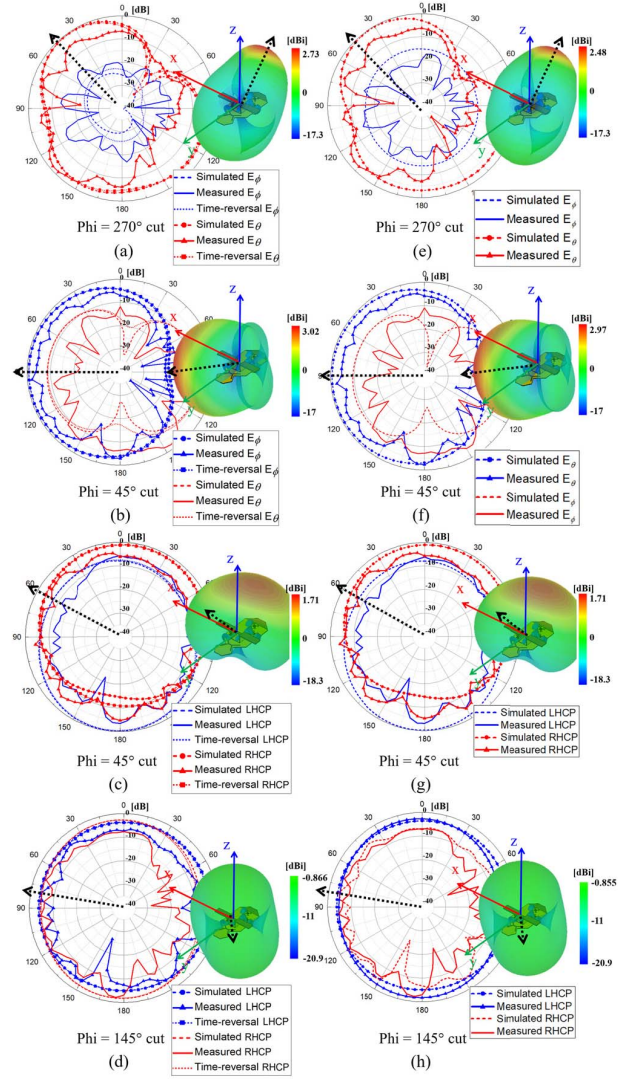


Fig. 6. (a)–(d) Radiation pattern results by the proposed algorithm using the impulse desired pattern. (e)–(h) Desired pattern considering the beam solid angle. (a) and (e) $(\theta_D, \phi_D) = (45^\circ, 270^\circ)$ with $(p_\theta, p_\phi) = (1, 0)$. (b) and (f) $(\theta_D, \phi_D) = (90^\circ, 45^\circ)$ with $(p_\theta, p_\phi) = (0, 1)$. (c) and (g) $(\theta_D, \phi_D) = (60^\circ, 45^\circ)$ with $(p_\theta, p_\phi) = (j, 1)$. (d) and (h) $(\theta_D, \phi_D) = (80^\circ, 145^\circ)$ with $(p_\theta, p_\phi) = (1, j)$. The 3-D patterns are the copolarized directivity patterns. The normalized phi-cut directivity patterns for all polarizations are plotted in polar coordinates.

an interval of 5° using the simulated three-port pattern matrix \mathbf{A}^{sim} . The left of Fig. 5 shows the results for the impulse desired pattern, and the right shows the results for the desired pattern considering the beam solid angle. The beam solid angle of the desired pattern used in the right was heuristically chosen as $(\pi/3)^2$. Because the weight vector of the proposed algorithm vanished at $\theta_D = 0^\circ$ or 180° owing to the $\sin(\theta_k)$ -weighted term in (18) and (21), the beam solid angle was chosen as $(\pi/36)^2$, particularly when θ_D is equal to 0° or 180° . Furthermore, the value of the desired angle θ_D was replaced with 0.5° and 179.5° when θ_D was equal to 0° or 180° . The results shown in Fig. 5 showed that beam steering worked well in most directions despite the synthesis of only three antenna patterns. The results near $\theta_D = 0^\circ$ or 180° were quite unstable for the desired pattern considering the beam solid angle because of the $\sin(\theta_k)$ -weighted term as mentioned above.

In identifying the overall shape of the synthesized pattern, the 3-D copodirectivity patterns and their 2-D phi-cut normalized patterns were plotted for the following cases marked with asterisks in Fig. 5: (1) $(\theta_D, \phi_D) = (45^\circ, 270^\circ)$ with $(p_\theta, p_\phi) = (1, 0)$; (2) $(\theta_D, \phi_D) = (90^\circ, 45^\circ)$ with $(p_\theta, p_\phi) = (0, 1)$; (3) $(\theta_D, \phi_D) = (60^\circ, 45^\circ)$ with $(p_\theta, p_\phi) = (j, 1)$; and (4) $(\theta_D, \phi_D) = (80^\circ, 145^\circ)$ with $(p_\theta, p_\phi) = (1, j)$. For each case, two results were basically compared: the results using the simulated three-port pattern matrix \mathbf{A}^{sim} and the measured three-port pattern matrix \mathbf{A}^{meas} provided in [18]. To start with, the impulse desired pattern mentioned in Section II-D was selected in Fig. 6(a)–(d). The results show that the copolarized patterns tend to be steered toward the desired direction except for the case shown in Fig. 6(c). In the case of Fig. 6(c), which is the worst case with RHCP shown in Fig. 5, it formed the gain to some extent toward the intended direction though the maximum gain direction deviated from the intended direction. For the results obtained using the measured three-port pattern matrix \mathbf{A}^{meas} , it did not follow the performance compared to the result using the simulated pattern matrix \mathbf{A}^{sim} because all three measured patterns tended to have a high gain in the direction of $\theta = 180^\circ$ in common due to the influence of the positioner and cable in the anechoic chamber. For some cases, this incomplete pattern produced the maximum gain around $\theta = 180^\circ$ not in the desired direction. Nevertheless, the tendency to perform beam steering to the desired direction was still maintained. The time-reversal processing results with twice full-wave simulation were compared in Fig. 6(a)–(d) to show the relationship between the proposed algorithm and the time-reversal processing. The plotted time-reversal results were obtained by simulating the model twice with the 3-D full-wave simulator, CST 2018 [20]. The first simulation provided the values for the received port signals when the plane-wave signal came from the desired direction. The second simulation provided the radiation pattern when the three-port antenna was excited with the weight as the ratio of the phase-conjugated received signals. As mentioned in Section II-C, the results for the impulse desired pattern were mostly consistent with those of the time-reversal processing when using the simulation pattern matrix \mathbf{A}^{sim} . Next, the desired pattern considering the beam solid angle mentioned was selected in Fig. 6(e)–(h) to evaluate the proposed algorithm for the same three cases. The beam solid angle of the desired pattern was heuristically chosen as $(\pi/3)^2$ same as the case shown in Fig. 5. For all cases, there was no significant difference from the cases of using the impulse desired pattern.

Nevertheless, the results shown in Figs. 5 and 6 imply some existing problems. First, the maximum gain at the desired direction ($\Delta_g = 0$) cannot be perfectly achieved for many angles because of the lack of the number of dominant CMs for this antenna design. Second, the axial ratio performance cannot be guaranteed because the proposed algorithm targets to maximize the copolarized gain and not suppress the cross-polarized gain. Finally, the results at the angle near $\theta = 0^\circ$ or 180° were slightly unstable because of the vanishing weighting vector by the $\sin(\theta)$ -weighted term.

IV. CONCLUSION

In this communication, a beamforming algorithm for a multiport chassis antenna was proposed using the LS method and the TCM. From the orthogonal properties of the CMs, the weighting vector for the desired direction and polarization can be easily obtained and analyzed in the physical point of view. The proposed algorithm only requires a multi-port antenna with the characteristics of decoupling

and pure CM generation; hence, it can be applied to any kind of multiport chassis antenna satisfying both characteristics. Although verification was provided with a multiport antenna model that only had three dominant CMs among the numerous examples, the proposed algorithm will be more likely to achieve a maximum gain in the desired direction if a multiport antenna has a more dominant CMs.

REFERENCES

- [1] S. Hwang, B. Lee, D. H. Kim, and J. Y. Park, "Design of S-band phased array antenna with high isolation using broadside coupled split ring resonator," *J. Electromagn. Eng. Sci.*, vol. 18, no. 2, pp. 108–116, Apr. 2018.
- [2] N. Yang, C. Caloz, and K. Wu, "Full-space scanning periodic phase-reversal leaky-wave antenna," *IEEE Trans. Microw. Theory Techn.*, vol. 58, no. 10, pp. 2619–2632, Oct. 2010.
- [3] S. V. S. Nair and M. J. Ammann, "Reconfigurable antenna with elevation and azimuth beam switching," *IEEE Antennas Wireless Propag. Lett.*, vol. 9, pp. 367–370, 2010.
- [4] Z. Li, E. Ahmed, A. M. Eltawil, and B. A. Cetiner, "A beam-steering reconfigurable antenna for WLAN applications," *IEEE Trans. Antennas Propag.*, vol. 63, no. 1, pp. 24–32, Jan. 2015.
- [5] Y. Yang and X. Zhu, "A wideband reconfigurable antenna with 360° beam steering for 802.11ac WLAN applications," *IEEE Trans. Antennas Propag.*, vol. 66, no. 2, pp. 600–608, Feb. 2018.
- [6] R. Harrington and J. Mautz, "Theory of characteristic modes for conducting bodies," *IEEE Trans. Antennas Propag.*, vol. AP-19, no. 5, pp. 622–628, Sep. 1971.
- [7] K. K. Kishor and S. V. Hum, "A pattern reconfigurable chassis-mode MIMO antenna," *IEEE Trans. Antennas Propag.*, vol. 62, no. 6, pp. 3290–3298, Jun. 2014.
- [8] Y. Chen and C.-F. Wang, "Electrically small UAV antenna design using characteristic modes," *IEEE Trans. Antennas Propag.*, vol. 62, no. 2, pp. 535–545, Feb. 2014.
- [9] Z. Liang, J. Ouyang, F. Yang, and L. Zhou, "Design of license plate RFID tag antenna using characteristic mode pattern synthesis," *IEEE Trans. Antennas Propag.*, vol. 65, no. 10, pp. 4964–4970, Oct. 2017.
- [10] F. A. Dicandia, S. Genovesi, and A. Monorchio, "Efficient excitation of characteristic modes for radiation pattern control by using a novel balanced inductive coupling element," *IEEE Trans. Antennas Propag.*, vol. 66, no. 3, pp. 1102–1113, Mar. 2018.
- [11] F. A. Dicandia, S. Genovesi, and A. Monorchio, "Advantageous exploitation of characteristic modes analysis for the design of 3-D null-scanning antennas," *IEEE Trans. Antennas Propag.*, vol. 65, no. 8, pp. 3924–3934, Aug. 2017.
- [12] F. A. Dicandia, S. Genovesi, and A. Monorchio, "Null-steering antenna design using phase-shifted characteristic modes," *IEEE Trans. Antennas Propag.*, vol. 64, no. 7, pp. 2698–2706, Jul. 2016.
- [13] H. Lebet and S. Boyd, "Antenna array pattern synthesis via convex optimization," *IEEE Trans. Signal Process.*, vol. 45, no. 3, pp. 526–532, Mar. 1997.
- [14] F. Wang, V. Balakrishnan, P. Y. Zhou, J. J. Chen, R. Yang, and C. Frank, "Optimal array pattern synthesis using semidefinite programming," *IEEE Trans. Signal Process.*, vol. 51, no. 5, pp. 1172–1183, May 2003.
- [15] F. Wang, R. Yang, and C. Frank, "A new algorithm for array pattern synthesis using the recursive least squares method," *IEEE Signal Process. Lett.*, vol. 10, no. 8, pp. 235–238, Aug. 2003.
- [16] L. Cen, Z. L. Yu, W. Ser, and W. Cen, "Linear aperiodic array synthesis using an improved genetic algorithm," *IEEE Trans. Antennas Propag.*, vol. 60, no. 2, pp. 895–902, Feb. 2012.
- [17] L. I. Vaskelainen, "Iterative least-squares synthesis methods for conformal array antennas with optimized polarization and frequency properties," *IEEE Trans. Antennas Propag.*, vol. 45, no. 7, pp. 1179–1185, Jul. 1997.
- [18] D.-W. Kim and S. Nam, "Systematic design of a multiport MIMO antenna with bilateral symmetry based on characteristic mode analysis," *IEEE Trans. Antennas Propag.*, vol. 66, no. 3, pp. 1076–1085, Mar. 2018.
- [19] The MathWorks. (2018). *MATLAB 2018a*. [Online]. Available: <https://www.mathworks.com>
- [20] CST Corporation. (2018). *CST Microwave Studio (MWS)*. [Online]. Available: <http://www.cst.com>